THE JOURNAL OF PHYSICAL CHEMISTRY A
A JOURNAL OF THE AMERICAN CHEMICAL SOCIETY

pubs.acs.org/JPCA Article

Substituent Effects on Torsional Strain in Cyclopentene Derivatives: A Computational Study

Brianna M. Coia, Luke A. Hudson, August J. Specht, III, and Justin G. Kennemur*

Cite This: J. Phys. Chem. A 2023, 127, 5005−5017 Read Online

ACCESS | Metrics & More | Article Recommendations | Supporting Information

ABSTRACT: Density functional theory calculations were used to create a library of ring strain energies (RSEs) for 73 cyclopentene derivatives with potential use as monomers for ring-opening metathesis polymerization (ROMP). An overarching goal was to probe how substituent choice may influence torsional strain, which is the driving force for ROMP and one of the most understudied types of RSEs. Potential trends investigated include substituent location, size, electronegativity, hybridization, and steric bulk. Using traditional and recently developed homodesmotic equations, our results show that the size and substitution (bulk) of the atom directly bonded to the ring have the greatest influence on torsional RSE. A complex interplay between bond length, bond angle, and dihedral angle dictates the relative eclipsed conformations between the substituent and its neighboring hydrogens and was found to be responsible for the notable differences in RSEs. Furthermore, substituents placed on the homoallylic position resulted in higher RSEs than the same substituent placed on the allylic position due to increased eclipsing interactions. Different levels of theory were also assessed, and it was determined that consideration of electron correlation in calculations increased RSEs by ∼2−5 kcal mol^{-1}. Further increasing the level of theory did not significantly change RSEs, indicating that the increased computational cost and time may not be necessary for improved accuracy.

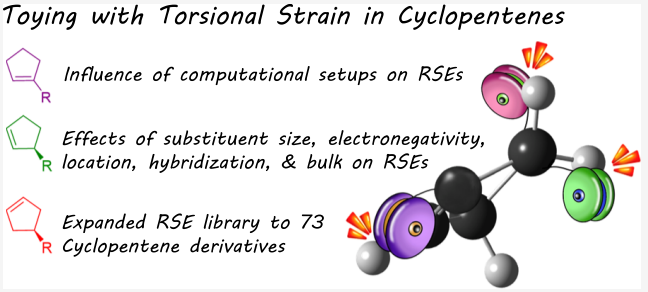

INTRODUCTION

Density functional theory (DFT) calculations have been useful in determining and studying ring strain energies (RSEs). Calculations for RSEs using homodesmotic reactions modeled after ring closing metathesis (RCM) have shown good agreement with the enthalpy of polymerization (ΔH_p) for the ring-opening metathesis polymerization (ROMP) of both cyclopentenes (CPs) and cyclooctenes.[1−7] For small-to-medium-sized rings, ΔH_p is usually the driving force for polymerization where RSE is commonly perceived as the dominant energetic term in ΔH_p.[8−11] Therefore, a better understanding of the complex relationships between substituents, structure, and RSE can facilitate and expedite the experimental design and synthesis of novel polymers.[1,3,4,9−12]

To date, most RSE investigations have focused on highly strained rings, rings with heteroatoms, and/or simple substituents (limited conformers).[4,5,13−26] As the number of atoms comprising the ring (n) increases, the source of RSE changes from predominantly angular (n = 3,4), to torsional (n = 5,6), to transannular (n = 7− ∼14) as shown in Figure 1.[9,27] The influence of various substituents on the ring can change the RSE. Angular strain is well studied and appears to follow Bent's Rule, which states that even small changes in hybridization can yield drastic differences in chemical properties, like RSE. This has been reflected in a variety of 3-membered rings ranging from hydrocarbon to heavy-element containing heterocycles.[16,28] Otherwise, RSE research has

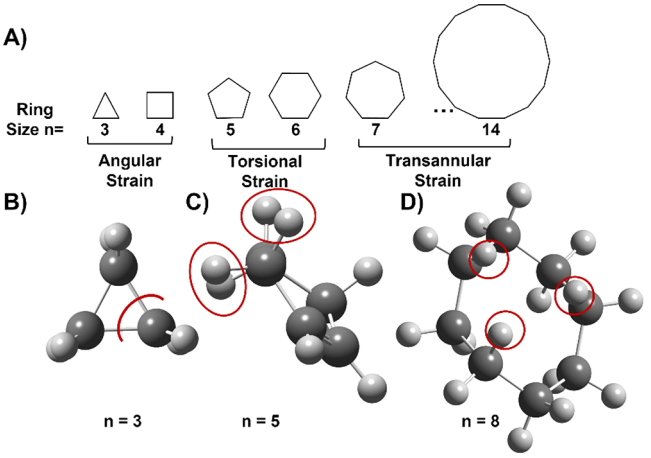

Figure 1. Types of ring strain energies (RSEs). (A) Strain categories as a function of ring size. Example of angular strain in cyclopropane (B), torsional strain in cyclopentene (C), and transannular strain in cyclooctane (D).

Received: April 5, 2023
Revised: May 10, 2023
Published: June 6, 2023

https://doi.org/10.1021/acs.jpca.3c02267
J. Phys. Chem. A 2023, 127, 5005−5017

Scheme 1. Homodesmotic Equations Used to Calculate RSEs[a]

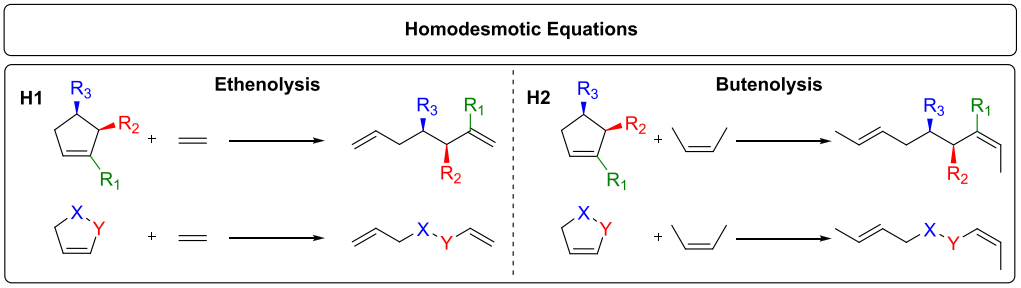

[a]Substituent locations (R) are denoted as alkenyl (R_1), allylic (R_2), or homoallylic (R_3). Heteroatom positions are represented by X (homoallylic), or Y (allylic).

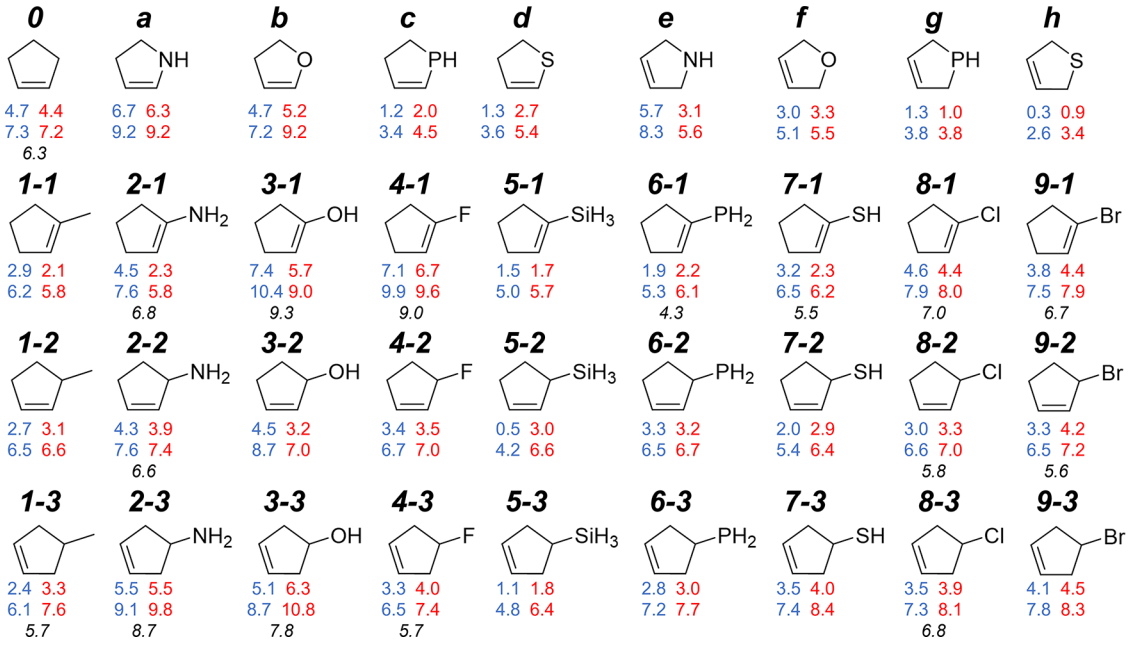

Figure 2. RSEs calculated with different levels of theory. Monomer ID is provided above its structure. Blue (left) and red (right) numbers were calculated with **H1** and **H2**, respectively. The top numbers (**Group 1**) are the average of RSEs calculated with B3LYP/6-31+G* and B3LYP/6-311++G**. Numbers below (**Group 2**) are the average of B3LYP-D3/6-31+G*, B3LYP-D3/6-311++G**, M06-2X/Def2-SVPP, M06-2X/Def2-QZVPP, M06-2X-D3/Def2-SVPP, and M06-2X-D3/Def2-QZVPP. Black bottom numbers were calculated using CBS-QB3 with **H1**. All averages had a standard deviation within ±1.2 kcal mol^{-1}.

centralized around complex bicyclic compounds (norbornanes, adamantanes, tetrahedranes, cubanes), which have a combination of the different strain types.[13,15,18,29] Studies regarding substituent effects have been limited to simple side chains and are usually either focused on angular and/or highly strained rings.[26,30−34]

Many of the exciting novel materials that can be synthesized via ROMP contain complex substituents, thus exhibiting a need to expand the library of available and comparable RSEs. Both CPs and cyclooctenes can bear a breadth of different substituents leading to an eclectic variety of possible materials. CPs have shown promise for chemically recyclable tire additives,[4] dynamic covalent networks,[35] and dynamic bottlebrush architectures by demonstrating high conversions for both polymerization and depolymerization.[36] Alternatively, the range of functionalities tested for cyclooctenes have yielded polymers with glass transition temperatures (T_g) ranging from −30 to 100 °C and thermal degradation temperatures (T_d) > 370 °C.[1] Further studies on *trans* fused cyclooctenes by Wang and co-workers showed that a narrow range of monomer RSEs (4.9−5.3 kcal mol^{-1}) was accompanied by ceiling temperatures (T_c) from 335 to 675 °C. The >300 °C range in T_c was attributed to subtle changes in fused ring size, stereochemistry, or substituent choice potentially highlighting the importance of considering the role of substituents (Thorpe-Ingold effect) even when not directly near the olefin.[3]

We recently found that RSE calculations for CPs using homodesmotic equations can be highly sensitive to conformational considerations, but RSEs calculated using a Boltzmann ensemble of conformers yielded negligible differences to RSEs calculated using only the low-energy conformers. RSEs also agreed well with previously reported ΔH_p values with a mean average deviation (MAD) and root-mean-square deviation (RMSD) of 0.97 and 1.22 kcal mol^{-1}, respectively, instilling confidence that more complex substituents can begin to be investigated using this method.[7] CPs are unique since they are the only monomer amenable to ROMP with RSEs dominated by torsional strain enabling a means to study the effects of complex substituents on the most understudied type of RSE. In this study, we expand the library of RSEs to 73 CP derivatives

https://doi.org/10.1021/acs.jpca.3c02267
J. Phys. Chem. A 2023, 127, 5005−5017

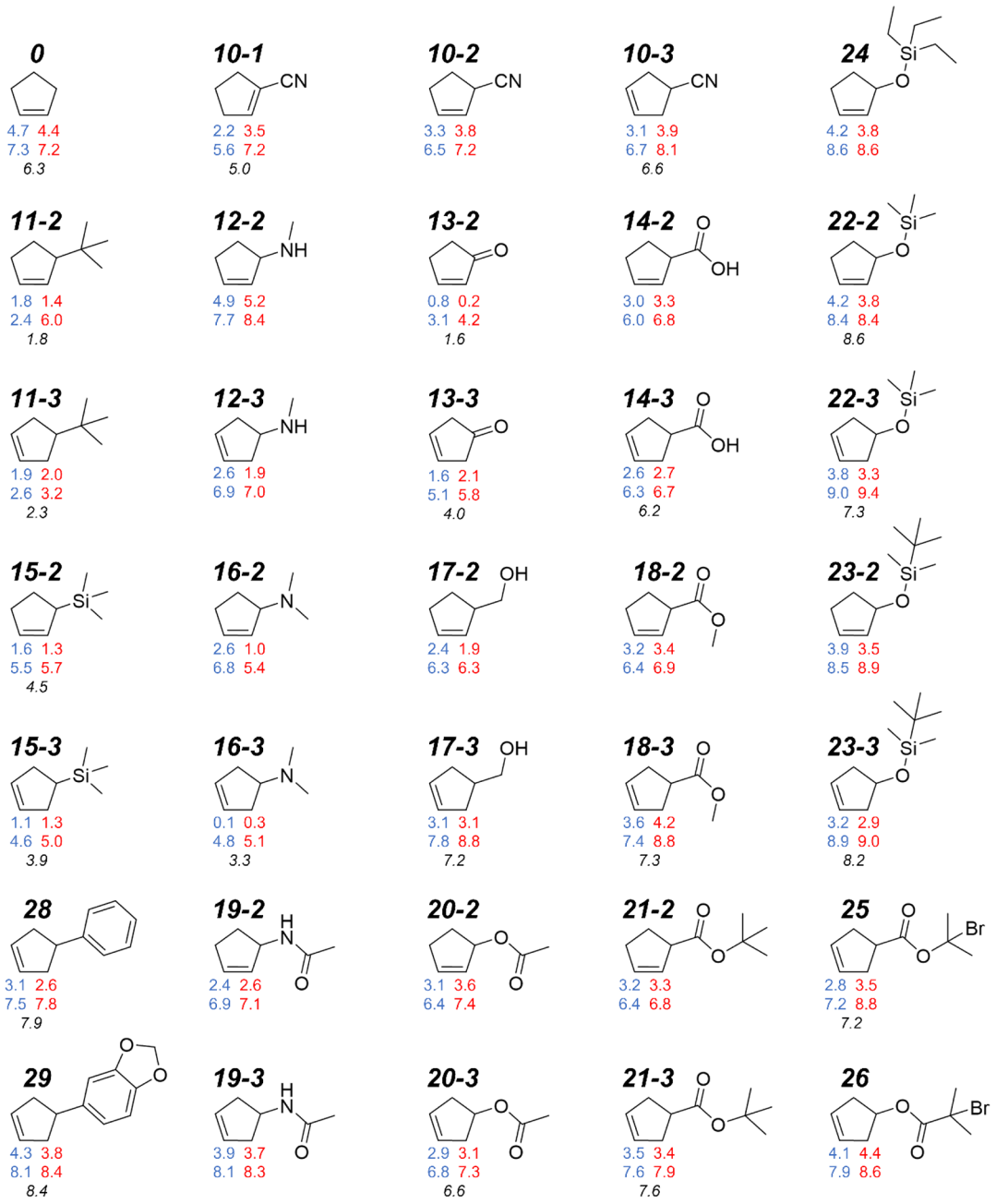

Figure 3. RSEs calculated with different levels of theory. Monomer ID is given above its structure. Blue (left) and red (right) numbers were calculated with **H1** and **H2**, respectively. The top numbers are the average of RSEs calculated with B3LYP/6-31+G* and B3LYP/6-311++G**. Numbers below are the average of B3LYP-D3/6-31+G*, B3LYP-D3/6-311++G**, M06-2X/Def2-SVPP, M06-2X/Def2-QZVPP, M06-2X-D3/Def2-SVPP, and M06-2X-D3/Def2-QZVPP. Black bottom numbers were calculated using CBS-QB3 with **H1**. All averages had a standard deviation within ±1.2 kcal mol^{-1}.

while simultaneously studying various potential substituent trends. The relationship between the substituents and RSE is probed via the effects of substituent location, hybridization, electronegativity, steric bulk, and atom size. Sensitivity of RSE values to the level of theory is also briefly explored. Levels of theory investigated include B3LYP[37,38] with 6-31+G* or 6-311++G**[39−45] as well as M06-2X[46] with Def2-SVPP or Def2-QZVPP[47] with and without the D3 dispersion correction.[48] Streamlined modulation of RSE via substituent choice can help facilitate and fine-tune reaction designs toward unique materials synthesized via not only ROMP, but potentially other ring-based transformations.

METHODS

RSE calculations were performed with G09 E.01,[49] GaussView 5.0,[50] and the homodesmotic equations shown in Scheme 1. Reaction Class 4 (RC4) homodesmotic equations were chosen because bond types, hybridizations, and substitutions are retained enabling more accurate representations of molecular connectivity and potential stereoelectronic effects.[51] The substituent location relative to the olefin was maintained between monomer and the linear analog. To keep potential stereoelectronics consistent, substituents were placed with stereoinversion next to the *cis* olefin in **H2** (Scheme 1). The levels of theory used include combinations of the hybrid

https://doi.org/10.1021/acs.jpca.3c02267
J. Phys. Chem. A 2023, 127, 5005−5017

generalized gradient approximation (GGA) functional, B3LYP,[37,38] the meta-GGA functional M06-2X,[46] and the D3 dispersion correction[48] with different basis sets. The basis sets chosen sample over small and large functions including the Pople basis sets (6-31+G* and 6-311++G**),[39−45] and Karlsruhe basis sets (Def2-SVPP and Def2-QZVPP)[47] for B3LYP and M06-2X, respectively. Optimizations were performed using B3LYP/6-31+G* and B3LYP/6-311++G** followed by frequency calculations to ensure that full convergence was achieved with zero imaginary frequencies within a local minimum on the potential energy surface (see the Supporting Information). Single point energy calculations were computed using B3LYP-D3 with the Pople basis sets, as well as M06-2X and M06-2X-D3 with the Karlsruhe basis sets. RSEs were calculated by adding the zero-point energy corrections (ZPE) from the B3LYP/6-311++G** frequency calculations to the total electronic energies (E) at the targeted level of theory (eq 1). Substituent hybridization was calculated using natural bonding orbital (NBO) analysis,[52] while steric bulk descriptors were calculated using the MORFEUS program[53] (see the Supporting Information).

$$\mathrm{RSE} = ((E_{\mathrm{acycle}} + \mathrm{ZPE}_{\mathrm{acycle}}) - (E_{\mathrm{cycle}} + E_{\mathrm{corr.factor}} + \mathrm{ZPE}_{\mathrm{cycle}} + \mathrm{ZPE}_{\mathrm{corr.factor}})) \quad (1)$$

RESULTS AND DISCUSSION

Homodesmotic eqs **H1** and **H2** (Scheme 1) were used to calculate the RSEs of 73 CP derivatives (Figures 2 and 3) using different levels of theory. For each monomer, a hyphenated sample ID was assigned where the first number is the functional group, and the second number represents the substituent location. Monomers were chosen via a combination of CPs commonly seen for ROMP as well as monomers that would provide a more thorough theoretical investigation of potential substituent influences on torsional strain.

Level of Theory. Before exploring substituent effects, the sensitivity of RSE values to the level of theory employed for the calculations was tested. Akin to experimental chemistry, theoretical RSE values depend on the model, techniques, and conditions employed.[13] For ROMP, one of the closer and more reasonably obtainable experimental values to compare theoretical values is the ΔH_p. It is worth emphasizing that RSE and ΔH_p are not the same value, but rather the RSE is believed to be the dominant energetic component of ΔH_p.[7,9−11] Studies that have compared RSEs to ΔH_p are typically calculated using the **H1** homodesmotic equation, which is modeled after ethenolysis and ring-opening of a monomer (Scheme 1). These calculations employed B3LYP/6-31G** and provided good agreement.[3,6,7] However, B3LYP is known to have limitations in calculating electron correlation energies, which depreciates the accuracy of larger molecules where midrange correlations are important.[48,54−57] Thermal corrections are also not reported in the previous calculations, suggesting room for improvement in the computational methods used to calculate these enthalpies.

To quickly probe potential variations in RSE values, a sampling of different levels of theory was assessed. A review of 200 functionals advised hybrid functionals for thermochemical predictions.[58] The semiempirical global hybrid generalized gradient approximation (GGA), B3LYP,[37,38] was compared to the semiempirical hybrid-meta GGA, M06-2X,[46] as it performed well with reasonable computational cost and time.[58−60] Grimme's D3 dispersion correction was also evaluated to bolster the description of long-range dynamic correlations.[58,61] A range of basis set sizes were also sampled from single to quadruple valence: 6-31+G*, 6-311++G**,[39−45] Def2-SVPP, and Def2-QZVPP.[62] Zero-point energy corrections (ZPE) from the B3LYP/6-311++G** frequency calculations were incorporated into the RSE calculations. The compound method CBS-QB3[63,64] was also investigated on a random sampling of monomers using **H1**. Since values between the more accurate DFT approaches did not vary considerably (MAD = 0.3 kcal mol^{-1}) from one of the more vetted but costly electronic structure methods, CBS-QB3, we decided to focus computational resources on the DFT methods (see the Supporting Information).

The most notable difference in RSEs is likely due to improved calculations of electron correlation energies as seen in Figures 2 and 3. The top numbers are the average of B3LYP and 6-31+G* or 6-311++G**(**Group 1**) where the mean absolute deviation (MAD) was 0.2 kcal mol^{-1} for **H1** and **H2**. The numbers below are the average of B3LYP-D3/6-31+G*, B3LYP-D3/6-311++G**, M06-2X/Def2-SVPP, M06-2X/Def2-QZVPP, M06-2X-D3/Def2-SVPP, and M06-2X-D3/Def2-QZVPP (**Group 2**) as to highlight a concise argument for the notable difference in RSEs upon improving the representation of electron correlations. Most RSEs computed in **Group 2** were within 2 kcal mol^{-1} for **H1** and **H2** with mean absolute deviations (MAD) of 0.5 kcal mol^{-1}. Regardless, even the lowest RSEs predicted in **Group 2** were ∼2−5 kcal mol^{-1} greater than in **Group 1**.

This distinct shift in RSEs can likely be attributed to error cancellation innate to homodesmotic equations. Systematic nonnegligible errors from functional and or/basis set limits have shown partial cancellation in homodesmotic equations.[54,57,65−68] We also recently found that olefin geometry, presented in the **H2** equations, can systematically shift RSEs by ∼2 kcal mol^{-1} depending on the relative numbers of *cis*/*trans* olefins on both sides of the equation.[7] Therefore, a similar phenomenon may be occurring within these calculations. B3LYP is known to ineffectively capture mid-to-long-range electron correlation energies, while the D3 correction can be used to address this shortcoming.[48,54−57] Upon adding the D3 correction to B3LYP, the RSEs immediately increase in value by ∼3−4 kcal mol^{-1} for both **H1** and **H2**. Contrarily, M06-2X was developed to improve calculations for weakly correlated systems.[69] Including the D3 correction did not significantly alter results as the MAD between M06-2X and M06-2X-D3 calculations was ≤ 0.7 kcal mol^{-1}. Therefore, slight considerations of electron correlation energies caused RSE calculations to nearly double in value, while further corrections did not significantly change results. Since the energies of the linear analogs in **H1** and **H2** would be more effected by changes in correlation terms compared to their monomers, the precipitous change in RSEs is likely due to a difference in error cancellation.

The basis set size had noticeably smaller influences on RSEs. Increasing the size of the basis set appeared to decrease RSE values. This is observed in comparing 6-31+G* to 6-311++G** and Def2-SVPP to Def2-QZVPP. Changing from a single to a double valence basis set yielded MADs ∼0.2 kcal mol^{-1}, while a single-to-quadruple valence increase in basis set size gave MADs ≤ 0.7 kcal mol^{-1}. In general, **H2** values are slightly higher than in **H1** suggesting that these methods may

https://doi.org/10.1021/acs.jpca.3c02267
J. Phys. Chem. A 2023, 127, 5005−5017

be less sensitive to olefin conformation than the methods previously reported.[7] We attribute the reduced sensitivity to the use of ZPE corrections, which allow for the estimation of electronic energy at 0 K, which theoretically is void of translational and rotational contributions.

Geometric Descriptors. As stated, the RSE of cyclopentene derivatives is mostly torsional due to the eclipsed nature of neighboring substituents on the sp^3 ring carbons.[9] Here, we note a substituent on the sp^2 olefin carbon (R_1) would be placed radially outward from the ring and less involved in torsional strain. Torsional strain is commonly described via the dihedral angle; however, a more holistic description of the relative proximity of vicinal groups appears to be necessary to understand the steric effects of more complex functional groups. To identify the origins of steric contributions to strain, the bond angle, dihedral angle, and bond length partaking in torsional repulsion were measured (Figure 4). For R_2 substituents (allylic) and R_3 substituents

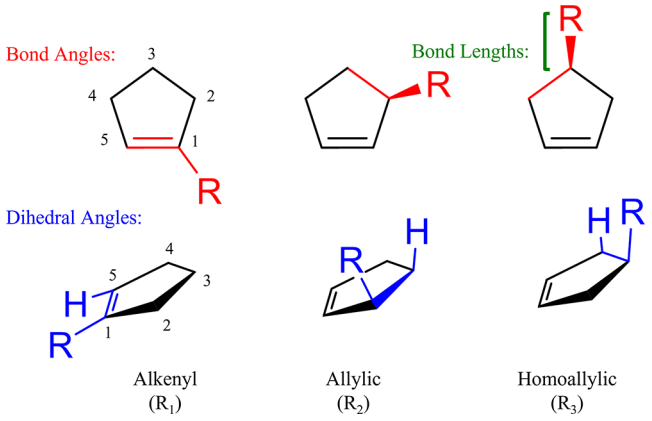

Figure 4. Geometric descriptors for torsional strain for alkenyl (R_1), allylic (R_2), and homoallylic (R_3) positions. Bond length (green), the C−R bond between substituent R and the monomer, as well as the bond (red) and dihedral (blue) angles help dictate the relative proximity between R and the eclipsing H.

(homoallylic), the bond angles of interest are C_3C_2R, and C_4C_3R (red, respectively) while the dihedral angles are HC_3C_2R and HC_4C_3R (blue, respectively). For context, a dihedral angle of 0° means perfect overlap (eclipsed) between the C−H and C−R bonds, which equates to the maximal steric repulsion possible, while 180° (anti) would provide maximal steric relief. The bond length is the C−R bond between the ring carbon in the CP monomer and the substituent (R). Overall, RSE appears to be complexly related to the bond angle, dihedral angle, and bond length that dictate the relative proximity of R to the neighboring H. This convoluted relationship also helps explain the observed outliers.

Substituent Location. The first RSE trend investigated is the position of the substituent relative to the olefin. Figure 5 shows the RSEs of 10 functional groups calculated at the alkenyl (R_1), allylic (R_2), and homoallylic (R_3) positions. Similarly, Figure 6 compares the R_2 to the R_3 substitution for 23 additional substituent groups. No clear trend is observed with the R_1 substitution; other than these RSEs appear to be the most sensitive to substituent chemistry detailed later in sections Atom Size and Electronegativity as well as Substituent Hybridization. The R_3 substitution yields slightly larger RSEs (~0.5−2 kcal mol^{-1}) than the R_2 position with some

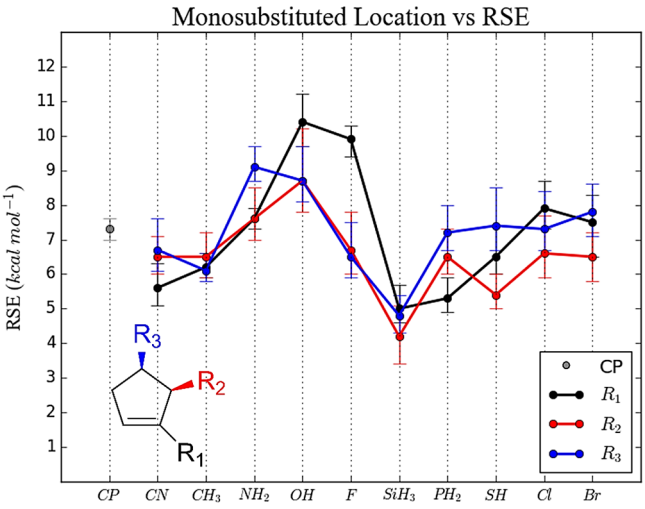

Figure 5. RSEs of monomers with varying substituent locations. Substituent locations are represented by black, red, and blue for R_1 (alkenyl), R_2 (allylic), and R_3(homoallylic), respectively. R is the functional group given along the *x*-axis. Unsubstituted CP is represented as a singular gray circle. RSEs are the average value from **Group 2** using **H1** with the error bars showing the range of RSEs calculated. Vertical dashed lines are used for visual guides.

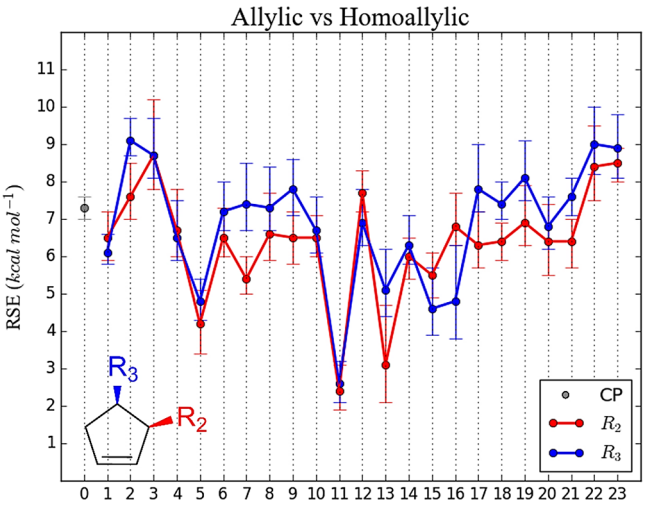

Figure 6. RSEs of monomers with varying substituent locations. R_2 (allylic) and R_3 (homoallylic) substituents are represented by red and blue, respectively. Values on the *x*-axis represent the first number in the sample IDs provided in Figures 2 and 3. Unsubstituted CP is represented as a singular gray circle. RSEs are the average value from **Group 2** using **H1** with the error bars showing the range of RSEs calculated. Vertical dashed lines are used for visual guides.

exceptions. For monomers with ~2 kcal mol^{-1} difference in RSE, there are no notable similarities between substituents **7** (sulfhydryl), **12** (*N*-methylamino), or **13** (carbonyl). The 5 monomers with higher RSEs in the allylic position also bear no distinct trend and include **1** (methyl), **4** (fluoro), **12** (*N*-methylamino), **15** (trimethylsilyl), and **16** (*N*,*N*-dimethylamino). The homoallylic position exhibited slightly higher strain because torsional strain is caused by the eclipsing of neighboring substituents. This is demonstrated by the increased steric repulsions experienced by homoallylic substituents due to the extra eclipsing interactions with the

https://doi.org/10.1021/acs.jpca.3c02267
J. Phys. Chem. A 2023, 127, 5005−5017

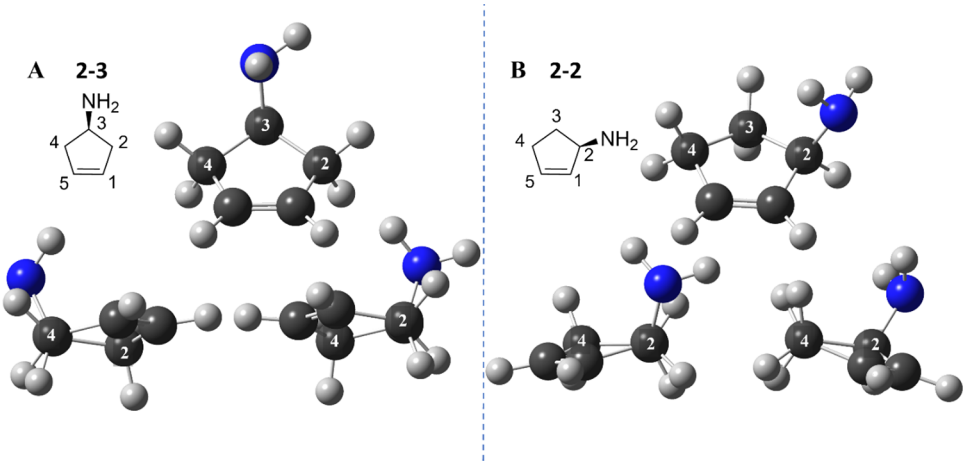

Figure 7. Eclipsing interactions in (A) homoallylic (R_3) and (B) allylic (R_2) amino-substituted CP (ID: **2-3** and **2-2**, respectively).The bottom views are along the C4−C3 and C2−C3 bonds.

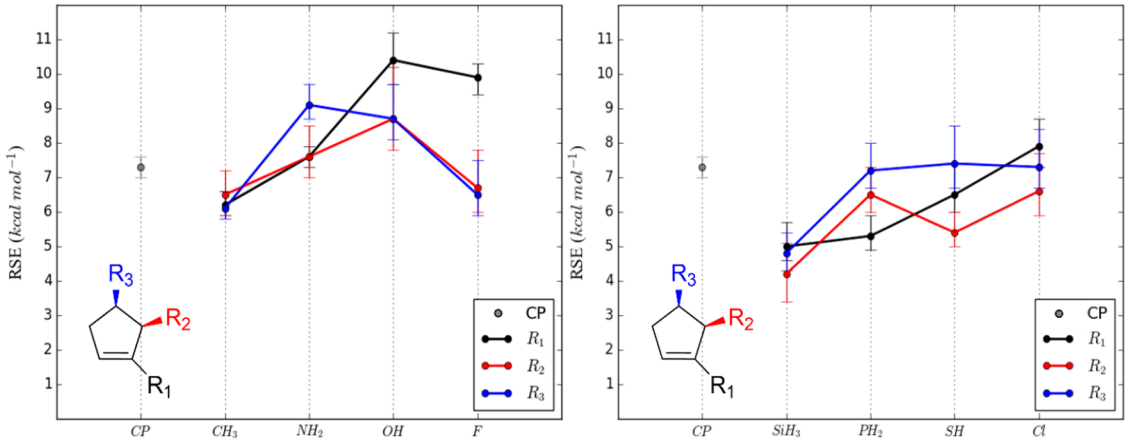

Figure 8. RSEs of monomers with period 2 (left) and 3 (right) elements as a function of increasing electronegativity. Alkenyl (R_1), allylic (R_2), and homoallylic (R_3) substitutions are represented by black, red, and blue, respectively. R is the functional group provided on the *x*-axis. Unsubstituted CP is represented as a singular gray circle. RSEs are the average value from **Group 2** using **H1** with the error bars showing the range of RSEs calculated. Vertical dashed lines are used for visual guides.

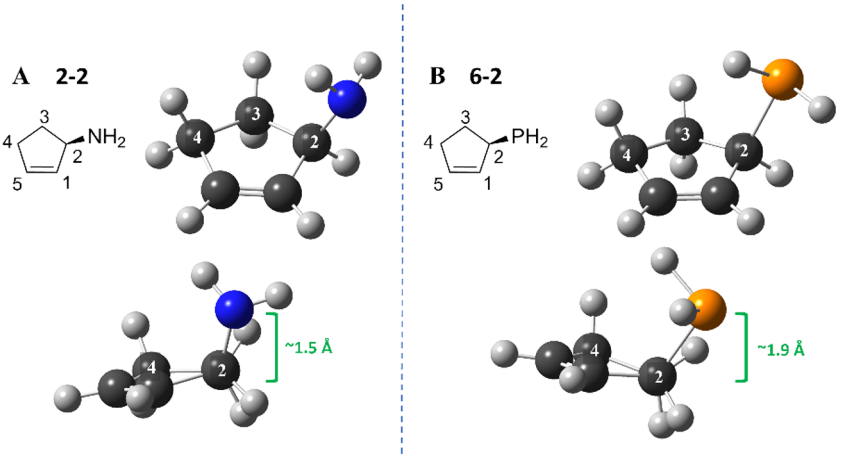

Figure 9. Difference in eclipsing due to increased bond length. A is **2-2**, while B is **6-2**. The bottom structures show the view along the C2−C3 bond. C−N and C−P bond lengths are given in green.

hydrogens on C2 and C4. In contrast, the allylic position only has the hydrogens on C3 (Figure 7).

Atom Size and Electronegativity. Investigating atom size and electronegativity revealed that larger atoms tend to exhibit ∼2 kcal mol^{-1} lower RSEs, while electronegativity did not show clear trends. Figure 8 shows RSEs as a function of both atom size and electronegativity with R_1, R_2, and R_3 substituent locations. Increasing the atom size from period 2

https://doi.org/10.1021/acs.jpca.3c02267
J. Phys. Chem. A 2023, 127, 5005−5017

(C, N, O, F) to period 3 (Si, P, S, Cl) in the periodic table caused a ∼2 kcal mol^{-1} decrease in RSE regardless of substituent location. The reduction in RSE is most likely due to the increased bond lengths to period 3 atoms. For example, Figure 9A displays the C−N bond length in **2-2** as ∼1.5 Å while the C-P (**6-2**) in Figure 9B is ∼1.9 Å, allowing for the PH_2 substituent to experience less steric repulsion with the neighboring hydrogens. The view along the C2−C3 bond in Figure 9 for **2-2** and **6-2** shows that the PH_2 substituent is notably less eclipsed with the neighboring methylene (C3) hydrogens. Electronegativity generally increases the RSE in the R_1 position, while the R_2 and R_3 substituents do not appear to follow a trend.

The halogens also show a unique behavior. F exhibits the only consistent decrease in RSE from the alkenyl to homoallylic position. While the allylic RSEs are the lowest for Cl and Br. The difference in F's behavior is most likely due to bond length. In the R_1 position (Figure 10, left column),

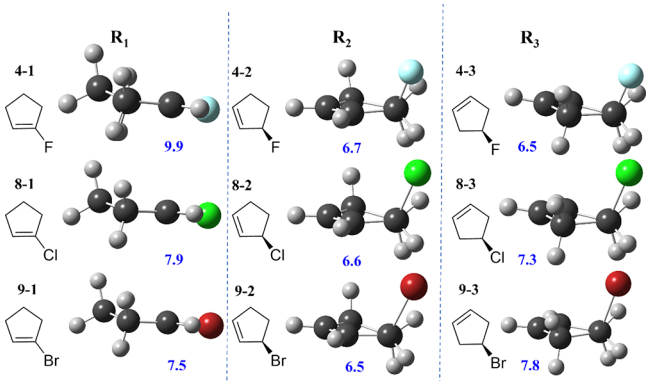

Figure 10. Relative eclipsing of halogens on the R_1, R_2, and R_3 positions. The halogens are F (top row, light blue), Cl (middle row, green), and Br (bottom row, red) with their monomer IDs above their structures. The average RSEs calculated from **Group 2** using **H1** are given in blue below their structures in kcal mol^{-1}.

RSE decreases noticeably (∼2 kcal mol^{-1}) from F to Cl and negligibly from Cl to Br (< 0.5 kcal mol^{-1}). The eclipsing shown in Figure 10 illustrates the likely cause of this drop in RSE. As the bond length increases from F (1.4 Å) to Br (1.9 Å), the eclipsing decreases as seen from the modeled side view of the rings. Note that the change in steric hinderance is more drastic from F to Cl than Cl to Br resembling the relative changes in RSEs. The R_2 substituents (Figure 10, middle column) have effectively no change in RSE, while R_3 (right column) interestingly displays an increase in RSE from F to Cl to Br, contradicting the prior arguments regarding bond length. The relative eclipsing of the halogens with their neighboring methylene hydrogens is consistent between the allylic and homoallylic monomers where F is the only notably eclipsed substituent. The askew eclipsing in allylic and homoallylic monomers is likely the cause for no distinct trends in RSEs for halogens and other common substituents.

When replacing ring carbons (C_2 or C_3) with heteroatoms nitrogen (a, e) oxygen (b, f), phosphorus (c, g), and sulfur (d, h), larger atoms reduce the RSE by ∼3 kcal mol^{-1} (Figure 11). Again, the increased bond lengths reduce eclipsing. Neighboring hydrogens are further away from the H bonded to P (∼2.6 Å) compared to CP (∼2.3 Å). The dihedrals in c (∼45°) and g (∼40°) are nearly double the dihedrals in CP (∼24°). The

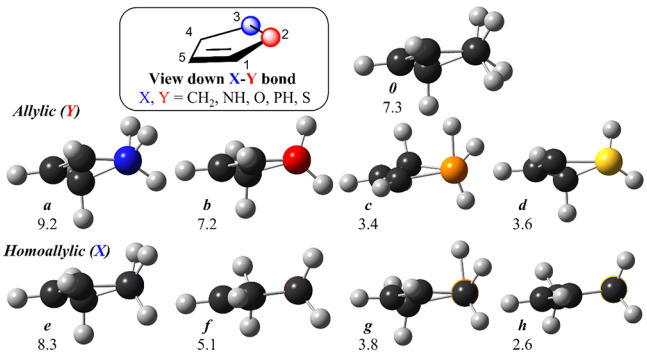

Figure 11. RSEs of monomers containing N, O, P, and S heteroatoms within the ring in place of the C_2 or C_3 carbon positions. Monomers are shown looking down the X−Y bond for 0, a−h. Heteroatoms are denoted by colors where N, O, P, and S are blue, red, orange, and yellow, respectively. Dark and light gray represent C and H, respectively. RSEs are the average value from **Group 2** using **H1**.

dihydrofurans (b, f) and dihydrothiophenes (d, h) are void of eclipsing H, which notably reduce the strain. The loss of eclipsing between both neighboring methylenes in f is the probable cause for the notably lower RSE than b. The dihydrothiazines (a, e) are interesting as they increase in RSE compared to CP. While the HC_2C_3H dihedral is larger (∼37°) in a, the HC_1C_2H dihedral decreases by ∼10° introducing eclipsing with the neighboring methine. It is worth noting that the lone pair would likely be engaging in steric repulsion with the methine as well. Overall, this suggests the source for the ∼2 kcal mol^{-1} net increase in RSE for the allylic position. In contrast, e has a reduction in dihedral by ∼10°, but only contains one hydrogen to eclipse supporting the slight increase in RSE.

Substituent Hybridization. Substituent hybridization has shown success in describing angular strain inspiring its investigation herein.[28] Hybridization describes the mixing of atomic orbitals (AOs) and is often simplified to sp^2- or sp^3-models. However, small changes in hybridization can yield notable differences in chemical properties, highlighting the need to accurately capture hybridization. In reality, the hybridization parameter (λ) in carbon sp^λ orbitals is better described as any range from a pure s($\lambda = 0$) to a pure p ($\lambda=\infty$) orbital. Therefore, a hybrid orbital can adopt between 0 and 100% of possible s or p characters. As carbon hybrid orbitals result from the mixing of one s and three p orbitals, their total characters respectively should summate to 100 and 300% for all occupied orbitals. Consequently, the orbital hybridization of the C−X bond is discussed in terms of %s and %p characters. Hybridization was determined using NBO analysis at the M06-2X-D3/Def2-QZVPP level of theory via SP calculations.

Analyzing the %s and %p characters of both the C and X atoms within the C−X bond yielded no significant correlations with RSE as illustrated in Figure 12. As expected, the %s and %p characters appear to be mirror images of each other. In general, the hybridization of the carbon atom incorporated in the parent cycle of the monomer appears to relate more with RSE than the first atom in the substituent, X. As %p increases (%s decreases), RSE generally increases for carbon, where there is no observable trend for the hybridization of X. These observations persist regardless of substituent location, and for RSEs computed using **H1** and **H2**. The lack of correlation is due to hybridization largely influencing molecular geometry, i.e., bond angles. Since CP strain is predominantly due to the

https://doi.org/10.1021/acs.jpca.3c02267
J. Phys. Chem. A 2023, 127, 5005−5017

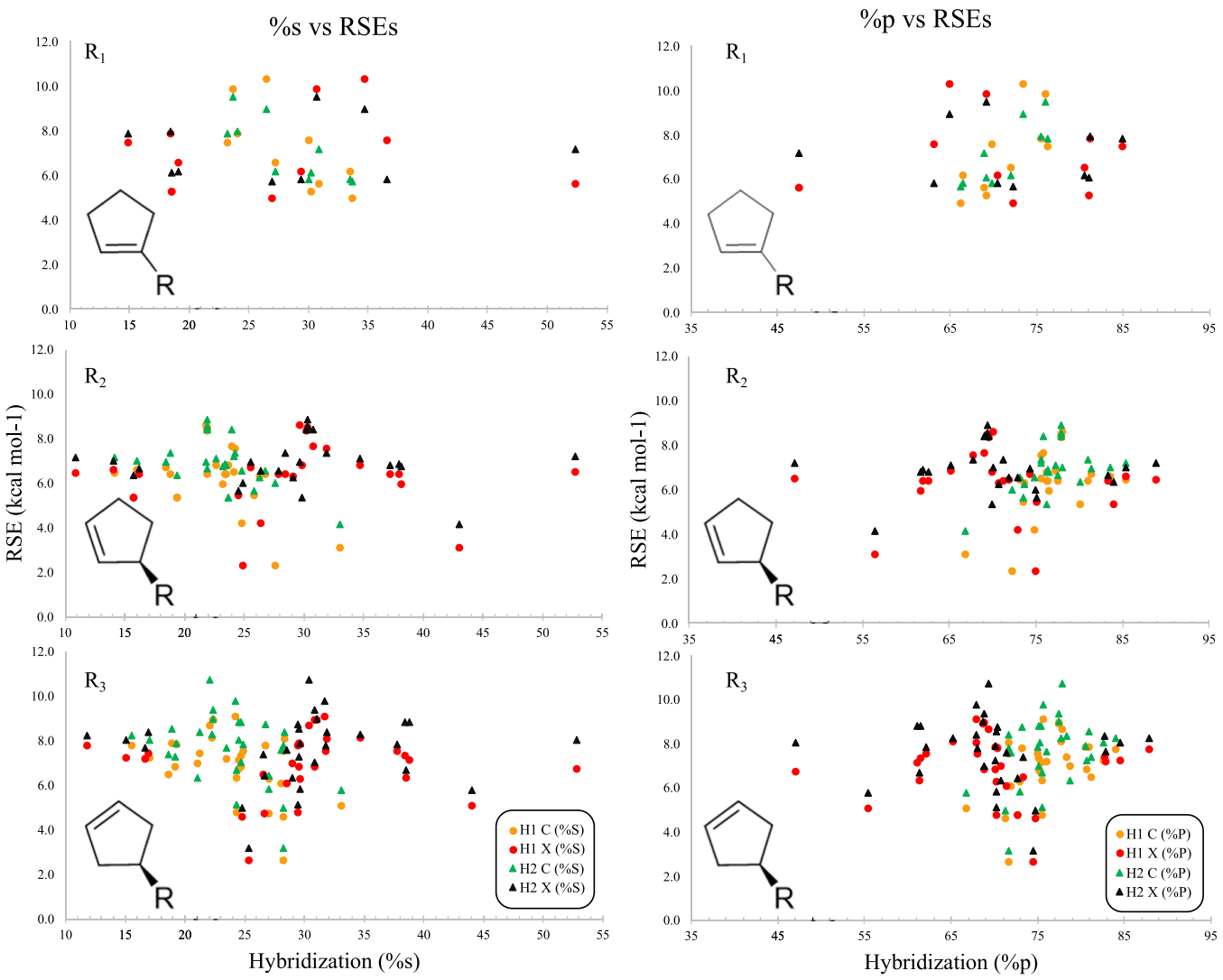

Figure 12. C−X hybridization compared to RSEs (kcal mol^{-1}) for different substituent locations R_1 (top), R_2 (middle), and R_3 (bottom). The %s character (left) and the %p character (right) are given for both C and X. RSEs are the average value from **Group 1** calculations using **H1** or **H2**. **H1** RSEs compared to C and X % characters are represented by yellow and red circles, respectively, while **H2** RSEs vs C and X % characters are illustrated by green and black triangles.

eclipsing of neighboring atoms, the RSEs should be independent of changes in hybridization.

Substituent Steric Bulk. Steric bulk is the main association for the Thorpe-Ingold effect. Steric bulk can be difficult to measure; however, Sterimol and the Tollman Cone Angle have been reported for use in comparing the sterics of ligands in catalysis.[53] We envisioned their use in gauging the relative steric bulk across the substituents studied herein. Sterimol parameters and cone angles were calculated using the open source MORFEUS program (Figure 13 and the Supporting Information).[53] The sterimol parameters calculated include L, B_1, and B_5, which effectively cover the length as well as the minimum and maximum rotational space of the substituent. The cone angle describes the space occupied from the first atom of the substituent relative to its maximum width (see the Supporting Information).

Steric bulk descriptors were compared to RSEs for all three substituent positions (Figure 13). L slightly decreased as RSE increased for R_1 monomers, while R_2 and R_3 monomer, L values were sporadic compared to RSE. The B_1 and B_5 parameters did not significantly change between most substituents, and therefore yielded no correlation with strain. The sterimol parameters do not describe the amount of bulk closest to the CP, but rather a holistic space occupied by the substituent. Therefore, we conclude that the lack of trends indicates that the influences of steric bulk become substantially less effective further from the CP. The most insightful steric bulk parameter was the cone angle, likely due to its better description of steric bulk closest to the CP. In general, the cone angles decreased with increasing RSEs supporting the idea that bulkier substituents favor RCM (smaller RSEs). However, it is worth noting that the cone angle did not provide a strong linear correlation ($R^2 \leq 0.3$). Collectively, these results suggest that increasing the distance of changes in steric bulk from the CP notably decreases the influences on strain.

A more scrutinous investigation was carried out on the effects of steric bulk only one atom from the parent cycle (Table 1). In most cases where the substituent location, bond angles and lengths, as well as dihedral angles are consistent RSEs remain similar. In both the allylic and homoallylic positions, the protecting groups trimethylsilyl (TMS) (**22**), *tert*-butyldimethylsilyl (TBS) (**23**), and triethylsilyl (TES)

https://doi.org/10.1021/acs.jpca.3c02267
J. Phys. Chem. A 2023, 127, 5005−5017

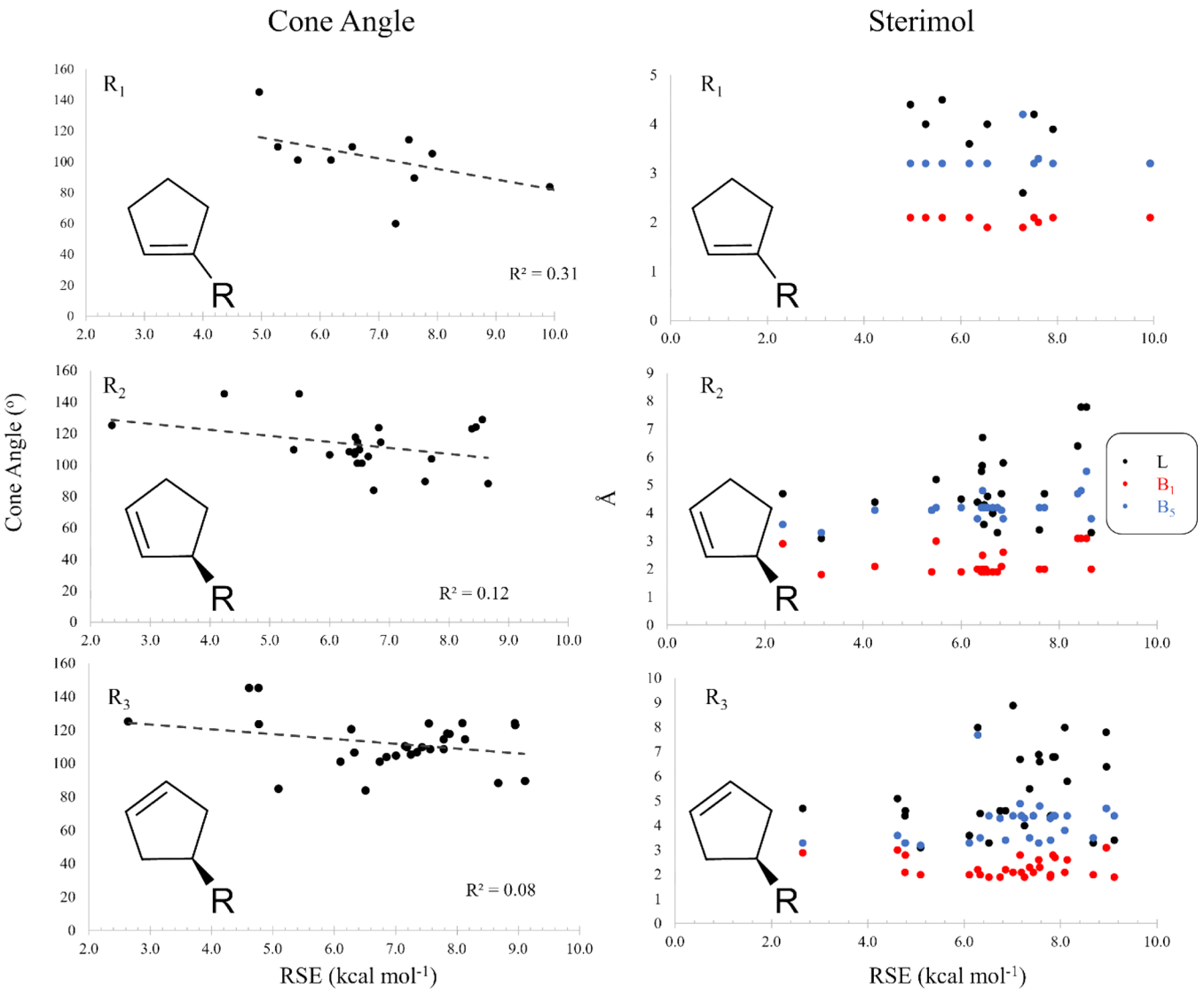

Figure 13. Steric bulk descriptors compared to RSEs for different substituent locations R_1 (top), R_2 (middle), and R_3 (bottom). Cone angles (left) are given in degrees (°), sterimol parameters (right) in angstrom (Å), and RSE in kcal mol^{-1}. Sterimol parameters L, B_1, and B_5 are black, red, and blue, respectively. RSEs are the average of **Group 1** using **H1**.

(**24**) exhibit no change in RSE (~8.5 and ~9.0 kcal mol^{-1}) mirroring the negligible differences in dihedral angles. The lack of change in RSE despite the changes in steric bulk suggests that steric contributions to strain quickly diminish after the atom directly bonded to the CP (Figure 14).

However, further application of this complex interplay between the bond angle, bond length, and dihedral angle did not consistently hold true (see the Supporting Information). Changing the substituent from **20**, **27**, to **26** yields RSEs of 6.8, 7.8, and 7.9 kcal mol^{-1}, respectively. Yet, the bond angles, lengths, and dihedrals of **20** and **26** are identical. The RSEs of **26** and **27** are almost identical despite the larger bond angle (~4°) and dihedral (~3°) in **27**. Similar stories are shown for the increase in bulk from **14**, **18**, **21**, and **25** in both allylic and homoallylic substituent locations further supporting that changes in steric bulk further from the cyclic parent minimally influence RSEs. Changes in the dihedral and bond angle also did not consistently explain observations for electronegativity or even switching substituent location. Therefore, these geometric descriptors are not robust enough to explain torsional strain across different atom types and substituent locations.

CONCLUSIONS

The RSEs of 73 CP derivatives were calculated to investigate the role of substituent location, size, electronegativity, hybridization, and bulk (Thorpe-Ingold effect) on torsional strain. Before substituent trends were analyzed, different computational setups were assessed. Interestingly, any level of consideration of electron correlation caused ~2−5 kcal mol^{-1} increase in RSEs. This was particularly highlighted by comparing B3LYP with and without Grimme's D3 dispersion correction. Further changes in calculating electron correlation did not notably change the RSEs as seen in comparing M06-2X with and without the D3 correction (MAD ≤ 0.7 kcal mol^{-1}). Most RSEs computed where electron correlation was considered were within 2 kcal mol^{-1} yielding a MAD = 0.5 kcal mol^{-1}. CBS-QB3 was also investigated for a random sampling of monomers but did not significantly vary from **Group 2** RSEs (MAD = 0.3 kcal mol^{-1}) suggesting that the

https://doi.org/10.1021/acs.jpca.3c02267
J. Phys. Chem. A 2023, 127, 5005−5017

Table 1. Geometric Descriptors for Steric Effects on Torsional Strain for R_2 (Allylic) and R_3 (Homoallylic) Monomers[a]

Monomer (R_2)	RSE (kcal mol^{-1})	Bond Angle (°)	Dihedral ngle (°)	Bond Length (Å)
0	7.3	109.3	23.8	1.1
1-2	6.5	113.7	19.7	1.5
5-2	4.2	113.7	23.5	1.9
11-2	2.4	116.2	−29.4	1.6
15-2	5.5	115.0	19.5	1.9
2-2	7.6	117.5	20.0	1.5
12-2	7.7	112.9	12.3	1.5
16-2	6.8	117.6	10.5	1.5
22-2	8.4	110.8	22.2	1.4
23-2	8.5	110.9	22.2	1.4
24	8.6	110.5	21.9	1.4
Monomer (R_3)	RSE (kcal mol^{-1})	Bond Angle (°)	Dihedral Angle (°)	Bond Length (Å)
0	7.3	109.3	23.8	1.1
1-3	6.1	114.6	−28.6	1.5
5-3	4.8	114.9	−28.2	1.9
11-3	2.6	116.4	−29.5	1.6
15-3	4.6	115.8	−28.5	1.9
2-3	9.1	109.2	20.9	1.5
12-3	6.9	113.2	−23.8	1.5
16-3	4.8	113.7	−28.7	1.5
22-3	9.0	112.2	26.9	1.4
23-3	8.9	113.2	26.5	1.4

[a]RSEs are the average of calculations performed with **H1** and **Group 2** given in kcal mol^{-1}. Geometric descriptors were obtained using B3LYP/6-311++G** geometries with the approach in Figure 12. The bond angle (BA), the dihedral angle (DA), and the cone angle (CA) are provided in degrees (°). Bond length (BL) refers to the C−R bond, where C is the carbon within the cyclopentene directly attached to substituent (R) given in Å.

increased accuracy is not worth the extra computational cost and time. Similarly, increasing the basis set size appeared to slightly decrease RSEs (MADs ≤ 0.7 kcal mol^{-1}). Therefore, slight considerations of electron correlation energies caused RSE calculations to nearly double in value, while further corrections did not significantly change results, and increasing computational accuracy did not warrant the increased cost and time as results remained similar.

The influence of the substituent on torsional strain appears to rely on a complex interplay between the bond length and angle as well as the dihedral angle that dictates the degree of eclipsing between the first atom of the substituent and its neighboring H's. The location, electronegativity, and hybridization of the substituent had less of an effect on RSE and prevented clear trends. In general, homoallylic substitution resulted in more eclipsing due to the extra neighboring methylene and therefore slightly larger RSEs than the allylic position. Hybridization of the C in the C-R substituent exhibited more correlation with RSE than R. As %p of C increased, the RSE generally increased. Steric bulk parameters L, B_1, and B_5 showed no significant trends, while the cone angle overall appears to be inversely related with RSE. More scrutinous investigations into the steric bulk and size of the first atom in the substituent elucidated that larger and more substituted first atoms typically decrease RSE. For larger atoms, decreased RSEs were attributed to decreased eclipsing in response to increased bond lengths. Greater substitutions of the first atom corresponded to a net decrease in eclipsing via a compromise between bond and dihedral angle, where the distance between R and its neighboring H's was overall increased. Changing the steric bulk after the first atom yielded no clear changes to RSE indicating that steric effects, such as the Thorpe-Ingold effect, are primarily important closest to the cyclic parent. Overall, the size and substitution of the first atom in the substituent appear to provide the best means to modulate monomer RSE in CPs, which can be used for rational monomer design moving forward. Between developing a facile, quick monomer screening method and elucidating how substituent choice may influence RSEs, we hope to reduce the cost, time, effort, and waste produced in the pursuit of high-value and more sustainable materials.

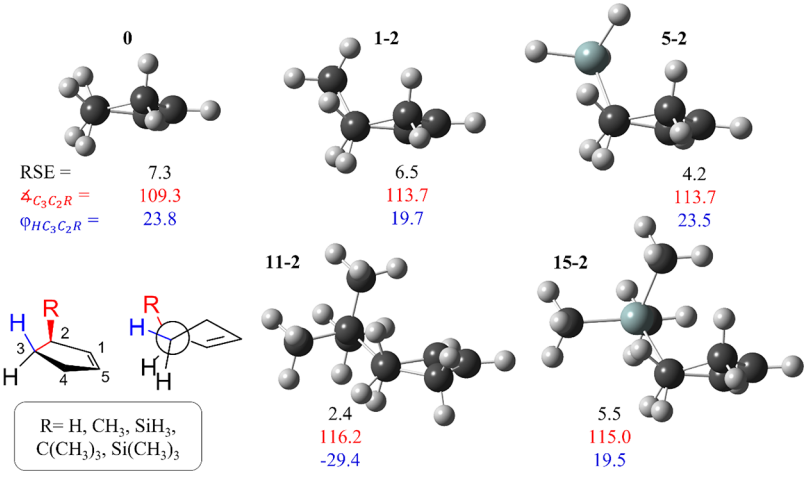

Figure 14. Steric bulk effects on geometric descriptors for torsional strain. Steric bulk increases from **0** (top left), **1-2** (top middle), **5-2**(top right), **11-2** (bottom left), to **15-2** (bottom right). Values include RSEs in kcal mol^{-1}, the bond angle (°), and dihedral angle (°) given in black, red, and blue, respectively. The bond angle is defined as C_3C_2R shown in red, and the dihedral angle is the bond angle plus the eclipsing hydrogen (HC_3C_2R) shown in blue.

https://doi.org/10.1021/acs.jpca.3c02267
J. Phys. Chem. A 2023, 127, 5005−5017

■ ASSOCIATED CONTENT

Data Availability Statement

The data that support the findings of this study are available from the corresponding author upon reasonable request.

Supporting Information

The Supporting Information is available free of charge at https://pubs.acs.org/doi/10.1021/acs.jpca.3c02267.

RSE calculations, **H2** substituent location vs RSE, **H2** size and electronegativity vs RSE, substituent hybridization, steric bulk descriptors, and structure coordinates (PDF)

■ AUTHOR INFORMATION

Corresponding Author

Justin G. Kennemur − *Department of Chemistry and Biochemistry, Florida State University, Tallahassee, Florida 32306, United States;* orcid.org/0000-0002-2322-0386; Email: jkennemur@fsu.edu

Authors

Brianna M. Coia − *Department of Chemistry and Biochemistry, Florida State University, Tallahassee, Florida 32306, United States*

Luke A. Hudson − *Department of Chemistry and Biochemistry, Florida State University, Tallahassee, Florida 32306, United States*

August J. Specht, III − *Department of Chemistry and Biochemistry, Florida State University, Tallahassee, Florida 32306, United States*

Complete contact information is available at: https://pubs.acs.org/10.1021/acs.jpca.3c02267

Notes

The authors declare no competing financial interest.

■ ACKNOWLEDGMENTS

This work was supported by the National Science Foundation under Grant Number 1750852. Calculations were performed using the Research Computing Center at Florida State University. We thank Letícia Madureira and Dr. Gabriel Gomes for helpful discussion.

■ REFERENCES

(1) Sathe, D.; Zhou, J.; Chen, H.; Su, H.-W.; Xie, W.; Hsu, T.-G.; Schrage, B. R.; Smith, T.; Ziegler, C. J.; Wang, J. Olefin metathesis-based chemically recyclable polymers enabled by fused-ring monomers. *Nat. Chem.* **2021**, *13*, 743−750.

(2) Chen, H.; Shi, Z.; Hsu, T.-G.; Wang, J. Overcoming the Low Driving Force in Forming Depolymerizable Polymers through Monomer Isomerization. *Angew. Chem., Int. Ed.* **2021**, *60*, 25493−25498.

(3) Zhou, J.; Sathe, D.; Wang, J. Understanding the Structure−Polymerization Thermodynamics Relationships of Fused-Ring Cyclooctenes for Developing Chemically Recyclable Polymers. *J. Am. Chem. Soc.* **2022**, *144*, 928−934.

(4) Tuba, R.; Balogh, J.; Hlil, A.; Barłóg, M.; Al-Hashimi, M.; Bazzi, H. S. Synthesis of Recyclable Tire Additives via Equilibrium Ring-Opening Metathesis Polymerization. *ACS Sustainable Chem. Eng.* **2016**, *4*, 6090−6094.

(5) Hlil, A. R.; Balogh, J.; Moncho, S.; Su, H.-L.; Tuba, R.; Brothers, E. N.; Al-Hashimi, M.; Bazzi, H. S. Ring opening metathesis polymerization (ROMP) of five- to eight-membered cyclic olefins: Computational, thermodynamic, and experimental approach. *J. Polym. Sci., Part A: Polym. Chem.* **2017**, *55*, 3137−3145.

(6) Hejl, A.; Scherman, O. A.; Grubbs, R. H. Ring-Opening Metathesis Polymerization of Functionalized Low-Strain Monomers with Ruthenium-Based Catalysts. *Macromolecules* **2005**, *38*, 7214−7218.

(7) Coia, B. M.; Werner, S. E.; Kennemur, J. G. Conformational bias in density functional theory ring strain energy calculations of cyclopentene derivatives: Towards predictive design of chemically recyclable elastomers. *J. Polym. Sci.* **2022**, *60*, 3391.

(8) Coates, G. W.; Getzler, Y. D. Y. L. Chemical recycling to monomer for an ideal, circular polymer economy. *Nat. Rev. Mater.* **2020**, *5*, 501−516.

(9) Neary, W. J.; Kennemur, J. G. Polypentenamer Renaissance: Challenges and Opportunities. *ACS Macro Lett.* **2019**, *8*, 46−56.

(10) Ivin, K. J.; Mol, J. C., *Olefin Metathesis and Metathesis Polymerization*. Academic Press: San Diego, CA, 1997.

(11) Ivin, K. J. Thermodynamics of addition polymerization. *J. Polym. Sci., Part A: Polym. Chem.* **2000**, *38*, 2137−2146.

(12) Neary, W. J.; Fultz, B. A.; Kennemur, J. G. Well-Defined and Precision-Grafted Bottlebrush Polypentenamers from Variable Temperature ROMP and ATRP. *ACS Macro Lett.* **2018**, *7*, 1080−1086.

(13) Rablen, P. R. A Procedure for Computing Hydrocarbon Strain Energies Using Computational Group Equivalents, with Application to 66 Molecules. *Chemistry* **2020**, *2*, 347−360.

(14) Dudev, T.; Lim, C. Ring Strain Energies from ab Initio Calculations. *J. Am. Chem. Soc.* **1998**, *120*, 4450−4458.

(15) Khoury, P. R.; Goddard, J. D.; Tam, W. Ring strain energies: substituted rings, norbornanes, norbornenes and norbornadienes. *Tetrahedron* **2004**, *60*, 8103−8112.

(16) Planells, A. R.; Ferao, A. E. Accurate Ring Strain Energy Calculations on Saturated Three-Membered Heterocycles with One Group 13−16 Element. *Inorg. Chem.* **2020**, *59*, 11503−11513.

(17) Wiberg, K. B.; Bonneville, G.; Dempsey, R. Strain Energies of Small Ring Alkenes. *Isr. J. Chem.* **1983**, *23*, 85−92.

(18) Schleyer, P. V. R.; Williams, J. E.; Blanchard, K. R. Evaluation of strain in hydrocarbons. The strain in adamantane and its origin. *J. Am. Chem. Soc.* **1970**, *92*, 2377−2386.

(19) Novak, I.; Chua, P. J. Computational Study of Pharmacophores: β-Lactams. *J. Phys. Chem. A* **2006**, *110*, 10521−10524.

(20) Lewis, L. L.; Turner, L. L.; Salter, E. A.; Magers, D. H. Computation of the conventional strain energy in oxaziridine. *J. Mol. Struct. Theochem.* **2002**, *592*, 161−171.

(21) Tuba, R.; Al-Hashimi, M.; Bazzi, H. S.; Grubbs, R. H. One-Pot Synthesis of Poly(vinyl alcohol) (PVA) Copolymers via Ruthenium Catalyzed Equilibrium Ring-Opening Metathesis Polymerization of Hydroxyl Functionalized Cyclopentene. *Macromolecules* **2014**, *47*, 8190−8195.

(22) Tuba, R.; Grubbs, R. H. Ruthenium catalyzed equilibrium ring-opening metathesis polymerization of cyclopentene. *Polym. Chem.* **2013**, *4*, 3959−3962.

(23) Al-Hashimi, M.; Tuba, R.; Bazzi, H. S.; Grubbs, R. H. Synthesis of Polypentenamer and Poly(Vinyl Alcohol) with a Phase-Separable Polyisobutylene-Supported Second-Generation Hoveyda−Grubbs Catalyst. *ChemCatChem* **2016**, *8*, 228−233.

(24) Hendrickson, J. B. Molecular Geometry. I. Machine Computation of the Common Rings. *J. Am. Chem. Soc.* **1961**, *83*, 4537−4547.

(25) Song, K.; Kim, K.; Hong, D.; Kim, J.; Heo, C. E.; Kim, H. I.; Hong, S. H. Highly active ruthenium metathesis catalysts enabling ring-opening metathesis polymerization of cyclopentadiene at low temperatures. *Nat. Commun.* **2019**, *10*, 3860.

(26) Confer, M. P.; Qu, T.; Rupar, P. A.; Dixon, D. A. Composite Correlated Molecular Orbital Theory Calculations of Ring Strain for Use in Predicting Polymerization Reactions. *ChemPhysChem* **2022**, *23*, No. e202200133.

(27) Anslyn, E. V.; Dougherty, D. A., *Modern physical organic chemistry*; University Science: Sausalito, CA, 2006.

(28) Alabugin, I. V.; Bresch, S.; Manoharan, M. Hybridization Trends for Main Group Elements and Expanding the Bent's Rule Beyond Carbon: More than Electronegativity. *J. Phys. Chem. A* **2014**, *118*, 3663−3677.
(29) Novak, I. Substituent effects on steric strain. *Chem. Phys. Lett.* **2003**, *380*, 258−262.
(30) Nagase, S.; Kobayashi, K.; Nagashima, M. Remarkable substituent effects on the strain energies of polycyclic silicon compounds. *J. Chem. Soc., Chem. Commun.* **1992**, 1302−1304.
(31) Fan, X.-W.; Ju, X.-H.; Xia, Q.-Y.; Xiao, H.-M. Strain energies of cubane derivatives with different substituent groups. *J. Hazard. Mater.* **2008**, *151*, 255−260.
(32) Bach, R. D.; Dmitrenko, O. Effect of Geminal Substitution on the Strain Energy of Dioxiranes. Origin of the Low Ring Strain of Dimethyldioxirane. *J. Org. Chem.* **2002**, *67*, 3884−3896.
(33) Lien, M. H.; Hopkinson, A. C. Substituent effects on the structures and strain energies of cyclopropenes. *J. Mol. Struct.Theochem.* **1987**, *149*, 139−151.
(34) Peverati, R.; Siegel, J. S.; Baldridge, K. K. Ab initio quantum chemical computations of substituent effects on triaziridine strain energy and heat of formation. *Phys. Chem. Chem. Phys.* **2009**, *11*, 2387−2395.
(35) Liu, H.; Nelson, A. Z.; Ren, Y.; Yang, K.; Ewoldt, R. H.; Moore, J. S. Dynamic Remodeling of Covalent Networks via Ring-Opening Metathesis Polymerization. *ACS Macro Lett.* **2018**, *7*, 933−937.
(36) Neary, W. J.; Isais, T. A.; Kennemur, J. G. Depolymerization of Bottlebrush Polypentenamers and Their Macromolecular Metamorphosis. *J. Am. Chem. Soc.* **2019**, *141*, 14220−14229.
(37) Becke, A. D. Density-functional exchange-energy approximation with correct asymptotic behavior. *Phys. Rev. A* **1988**, *38*, 3098−3100.
(38) Lee, C.; Yang, W.; Parr, R. G. Development of the Colle-Salvetti correlation-energy formula into a functional of the electron density. *Phys. Rev. B* **1988**, *37*, 785−789.
(39) Ditchfield, R.; Hehre, W. J.; Pople, J. A. Self-Consistent Molecular-Orbital Methods. IX. An Extended Gaussian-Type Basis for Molecular-Orbital Studies of Organic Molecules. *J. Chem. Phys.* **1971**, *54*, 724−728.
(40) Hehre, W. J.; Ditchfield, R.; Pople, J. A. Self—Consistent Molecular Orbital Methods. XII. Further Extensions of Gaussian—Type Basis Sets for Use in Molecular Orbital Studies of Organic Molecules. *J. Chem. Phys.* **1972**, *56*, 2257−2261.
(41) Hariharan, P. C.; Pople, J. A. The influence of polarization functions on molecular orbital hydrogenation energies. *Theor. Chim. Acta* **1973**, *28*, 213−222.
(42) Krishnan, R.; Binkley, J. S.; Seeger, R.; Pople, J. A. Self-consistent molecular orbital methods. XX. A basis set for correlated wave functions. *J. Chem. Phys.* **1980**, *72*, 650−654.
(43) Francl, M. M.; Pietro, W. J.; Hehre, W. J.; Binkley, J. S.; Gordon, M. S.; DeFrees, D. J.; Pople, J. A. Self-consistent molecular orbital methods. XXIII. A polarization-type basis set for second-row elements. *J. Chem. Phys.* **1982**, *77*, 3654−3665.
(44) Clark, T.; Chandrasekhar, J.; Spitznagel, G. W.; Schleyer, P. V. R. Efficient diffuse function-augmented basis sets for anion calculations. III. The 3−21+G basis set for first-row elements, Li−F. *J. Comput. Chem.* **1983**, *4*, 294−301.
(45) Frisch, M. J.; Pople, J. A.; Binkley, J. S. Self-consistent molecular orbital methods 25. Supplementary functions for Gaussian basis sets. *J. Chem. Phys.* **1984**, *80*, 3265−3269.
(46) Zhao, Y.; Truhlar, D. G. The M06 suite of density functionals for main group thermochemistry, thermochemical kinetics, noncovalent interactions, excited states, and transition elements: two new functionals and systematic testing of four M06-class functionals and 12 other functionals. *Theor. Chem. Acc.* **2008**, *120*, 215−241.
(47) Weigend, F.; Ahlrichs, R. Balanced basis sets of split valence, triple zeta valence and quadruple zeta valence quality for H to Rn: Design and assessment of accuracy. *Phys. Chem. Chem. Phys.* **2005**, *7*, 3297−3305.
(48) Grimme, S.; Antony, J.; Ehrlich, S.; Krieg, H. A consistent and accurate ab initio parametrization of density functional dispersion correction (DFT-D) for the 94 elements H-Pu. *J. Chem. Phys.* **2010**, *132*, 154104.
(49) Frisch, M. J.; Trucks, G. W.; Schlegel, H. B.; Scuseria, G. E.; Robb, M. A.; Cheeseman, J. R.; Scalmani, G.; Barone, V.; Petersson, G. A.; Nakatsuji, H.; Li, X.; Caricato, M.; Marenich, A. V.; Bloino, J.; Janesko, B. G.; Gomperts, R.; Mennucci, B.; Hratchian, H. P.; Ortiz, J. V.; Izmaylov, A. F.; Sonnenberg, J. L.; Williams; Ding, F.; Lipparini, F.; Egidi, F.; Goings, J.; Peng, B.; Petrone, A.; Henderson, T.; Ranasinghe, D.; Zakrzewski, V. G.; Gao, J.; Rega, N.; Zheng, G.; Liang, W.; Hada, M.; Ehara, M.; Toyota, K.; Fukuda, R.; Hasegawa, J.; Ishida, M.; Nakajima, T.; Honda, Y.; Kitao, O.; Nakai, H.; Vreven, T.; Throssell, K.; Montgomery, Jr., J. A.; Peralta, J. E.; Ogliaro, F.; Bearpark, M. J.; Heyd, J. J.; Brothers, E. N.; Kudin, K. N.; Staroverov, V. N.; Keith, T. A.; Kobayashi, R.; Normand, J.; Raghavachari, K.; Rendell, A. P.; Burant, J. C.; Iyengar, S. S.; Tomasi, J.; Cossi, M.; Millam, J. M.; Klene, M.; Adamo, C.; Cammi, R.; Ochterski, J. W.; Martin, R. L.; Morokuma, K.; Farkas, O.; Foresman, J. B.; Fox, D. J. *Gaussian 09 E.01*(Gaussian, Inc.), Wallingford, CT, 2013
(50) Nielsen, A. B.; Holder, A. J., GaussView 5.0, *User's Reference.* (Gaussian, Inc.) Pittsburgh, PA., 2009.
(51) Wheeler, S. E.; Houk, K. N.; Schleyer, P. V. R.; Allen, W. D. A Hierarchy of Homodesmotic Reactions for Thermochemistry. *J. Am. Chem. Soc.* **2009**, *131*, 2547−2560.
(52) Glendening, E. D.; Reed, A. E.; Carpenter, J. E.; Weinhold, F., *NBO Version 3.1*.
(53) Gensch, T.; dos Passos Gomes, G.; Friederich, P.; Peters, E.; Gaudin, T.; Pollice, R.; Jorner, K.; Nigam, A.; Lindner-D'Addario, M.; Sigman, M. S.; Aspuru-Guzik, A. A Comprehensive Discovery Platform for Organophosphorus Ligands for Catalysis. *J. Am. Chem. Soc.* **2022**, *144*, 1205−1217.
(54) Redfern, P. C.; Zapol, P.; Curtiss, L. A.; Raghavachari, K. Assessment of Gaussian-3 and Density Functional Theories for Enthalpies of Formation of C1−C16 Alkanes. *J. Phys. Chem. A* **2000**, *104*, 5850−5854.
(55) Zhang, I. Y.; Wu, J.; Xu, X. Extending the reliability and applicability of B3LYP. *Chem. Commun.* **2010**, *46*, 3057−3070.
(56) Krieg, H.; Grimme, S. Thermochemical benchmarking of hydrocarbon bond separation reaction energies: Jacob's ladder is not reversed! *Mol. Phys.* **2010**, *108*, 2655−2666.
(57) Tirado-Rives, J.; Jorgensen, W. L. Performance of B3LYP Density Functional Methods for a Large Set of Organic Molecules. *J. Chem. Theory Comput.* **2008**, *4*, 297−306.
(58) Mardirossian, N.; Head-Gordon, M. Thirty years of density functional theory in computational chemistry: an overview and extensive assessment of 200 density functionals. *Mol. Phys.* **2017**, *115*, 2315−2372.
(59) Goerigk, L.; Grimme, S. A thorough benchmark of density functional methods for general main group thermochemistry, kinetics, and noncovalent interactions. *Phys. Chem. Chem. Phys.* **2011**, *13*, 6670−6688.
(60) Wheeler, S. E.; Moran, A.; Pieniazek, S. N.; Houk, K. N. Accurate Reaction Enthalpies and Sources of Error in DFT Thermochemistry for Aldol, Mannich, and α-Aminoxylation Reactions. *J. Phys. Chem. A* **2009**, *113*, 10376−10384.
(61) Burns, L. A.; Mayagoitia, Á. V.; Sumpter, B. G.; Sherrill, C. D. Density-functional approaches to noncovalent interactions: A comparison of dispersion corrections (DFT-D), exchange-hole dipole moment (XDM) theory, and specialized functionals. *J. Chem. Phys.* **2011**, *134*, No. 084107.
(62) Rappoport, D.; Furche, F. Property-optimized Gaussian basis sets for molecular response calculations. *J. Chem. Phys.* **2010**, *133*, 134105.
(63) Montgomery, J. A.; Frisch, M. J.; Ochterski, J. W.; Petersson, G. A. A complete basis set model chemistry VI. Use of density functional geometries and frequencies. *J. Chem. Phys.* **1999**, *110*, 2822−2827.
(64) Montgomery, J. A.; Frisch, M. J.; Ochterski, J. W.; Petersson, G. A. A complete basis set model chemistry. VII. Use of the minimum

https://doi.org/10.1021/acs.jpca.3c02267
J. Phys. Chem. A 2023, 127, 5005−5017

population localization method. *J. Chem. Phys.* **2000**, *112*, 6532−6542.
(65) Houk, K. N.; Liu, F. Holy Grails for Computational Organic Chemistry and Biochemistry. *Acc. Chem. Res.* **2017**, *50*, 539−543.
(66) Grimme, S. n-Alkane Isodesmic Reaction Energy Errors in Density Functional Theory Are Due to Electron Correlation Effects. *Org. Lett.* **2010**, *12*, 4670−4673.
(67) van Speybroeck, V.; Gani, R.; Meier, R. J. The calculation of thermodynamic properties of molecules. *Chem. Soc. Rev.* **2010**, *39*, 1764−1779.
(68) van Duijneveldt, F. B.; van Duijneveldt-van de Rijdt, J. G. C. M.; van Lenthe, J. H. State of the Art in Counterpoise Theory. *Chem. Rev.* **1994**, *94*, 1873−1885.
(69) Wang, Y.; Verma, P.; Jin, X.; Truhlar, D. G.; He, X. Revised M06 density functional for main-group and transition-metal chemistry. *Proc. Natl. Acad. Sci. U. S. A.* **2018**, *115*, 10257.

https://doi.org/10.1021/acs.jpca.3c02267
J. Phys. Chem. A 2023, 127, 5005−5017